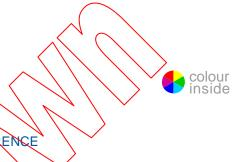


Edition 3.1 2012-07

# TECHNICAL REPORT



INTERNATIONAL SPECIAL COMMITTEE ON RADIO INTERFERENCE

Specification for radio disturbance and immunity measuring apparatus and methods –

Part 3: CISPR technical reports



INTERNATIONAL ELECTROTECHNICAL COMMISSION

ICS 33.100.10, 33.100.20 ISBN 978-2-8322-0282-1

Warning! Make sure that you obtained this publication from an authorized distributor.

## CONTENTS

FC	REW	)RD		14	
1	Scop	Scope			
2	Norm	native re	eferences	16	
3	Term	ıs, defir	nitions and abbreviations	17	
	3.1	Terms	and definitions	17	
	3.2	Abbre	viations	20	
4	Tech	nical re	ports	20	
	4.1	charac	ation between measurements made with apparatus having cteristics differing from CISPR characteristics and measurements made	20	
		4.1.1	General	20	
		4.1.2	Critical interference-measuring instrument parameters	21	
		4.1.3	Impulse interference – correlation factors	23	
		4.1.4	Random noise	25	
		4.1.5	The root mean square (rms) detector	25	
		4.1.6	Discussion	25	
		4.1.7	Application to typical noise sources	25	
		4.1.8	Conclusions		
	4.2	Interfe	erence simulators	27	
		4.2.1	General	27	
		4.2.2	Types of interference signals		
		4.2.3	Circuits for simulating broadband interference	28	
	4.3		onship between limits for open-area test site and the reverberation	20	
			Der		
		4.3.1 4.3.2	General  Correlation between measurement results of the reverberation	32	
			chamber and OATS		
		4.3.3	Limits for use with the reverberation chamber method		
		4.3.4	Rrocedure for the determination of the reverberation chamber limit	33	
	4.4	induce	cterization and classification of the asymmetrical disturbance source ad in telephone subscriber lines by AM broadcasting transmitters in the liw and SW bands	34	
		4.4.1	General		
		4.4.2	Experimental characterization	34	
		4.4.3	Prediction models and classification	44	
		4.4.4	Characterization of the immunity-test disturbance source	47	
	4.5	Predic	tability of radiation in vertical directions at frequencies above 30 MHz	55	
		4.5.1	Summary	55	
		4.5.2	Range of application	56	
		4.5.3	General	56	
		4.5.4	Method used to calculate field patterns in the vertical plane	58	
		4.5.5	Limitations of predictability of radiation at elevated angles	59	
		4.5.6	Differences between the fields over a real ground and the fields over a perfect conductor	87	
		4.5.7	Uncertainty ranges		
		4.5.8	Conclusions	96	

4.6		edictability of radiation in vertical directions at frequencies up to z	97
	4.6.1	Range of application	
	4.6.2	General	
	4.6.3	Method of calculation of the vertical radiation patterns	
	4.6.4	The source models	
	4.6.5	Electrical constants of the ground	
	4.6.6	Predictability of radiation in vertical directions	
	4.6.7	Conclusions	
	4.6.8	Figures associated with predictability of radiation in vertical directions	
4.7		ation between amplitude probability distribution (APD) characteristics urbance and performance of digital communication systems	139
	4.7.1	General	
	4.7.2	Influence on a wireless LAN system	139
	4.7.3	Influence on a Bluetooth system	142
	4.7.4	Influence on a W-CDMA system	146
	4.7.5	Influence on Personal Handy Phone System (PHS)	149
	4.7.6	Quantitative correlation between noise parameters and system performance	153
	4.7.7	Quantitative correlation between noise parameters of repetition pulse and system performance of RHS and W-CDMA (BER)	157
4.8		round material on the definition of the rms-average weighting detector asuring receivers	
	4.8.1	General purpose of weighted measurement of disturbance	160
	4.8.2	General principle of weighting the CISPR quasi-peak detector	
	4.8.3	Other detectors defined in CISPR 16-1-1	
	4.8.4	Procedures for measuring pulse weighting characteristics of digital radjocommunications services	162
	4.8.5	Theoretical studies	
	4.8.6	Experimental results.	
	4.8.7	Effects of spread-spectrum clock interference on wideband radiocommunication signal reception	185
	4.8.8	Analysis of the various weighting characteristics and proposal of a	
<		weighting detector	186
	4.8.9	Properties of the rms-average weighting detector	189
4.9	Comm	on mode absorption devices (CMAD)	191
	4.9.1	General	191
	4.9.2	CMAD as a two-port device	193
	4.9.3	Measurement of CMAD	197
4.10	Backgı	round on the definition of the FFT-based receiver	207
	4.10.1	General	207
	4.10.2	Tuned selective voltmeters and spectrum analyzers	208
	4.10.3	General principle of a tuned selective voltmeter	208
	4.10.4	FFT-based receivers – digital signal processing	210
	4.10.5	Measurement errors specific to FFT processing	213
	4.10.6	FFT-based receivers – examples	215
4.11		eters of signals at telecommunication ports	
	4.11.1	General	228
	4 11 2	Estimation of common mode disturbance levels	230

5	Back	ground	and h	istory of CISPR	231
	5.1	The his	story o	of CISPR	231
		5.1.1	The	early years: 1934-1984	231
		5.1.2	The	division of work	233
		5.1.3	The	computer years: 1984 to 1998	233
		5.1.4	The	people in CISPR	233
	5.2	power	produ	ckground to the method of measurement of the interference ced by electrical household and similar appliances in the VHF	22.4
		5.2.1		orical detail	234
		5.2.1		elopment of the method	
Anr	nex A	·		Derivation of the formula	237
		•		The field-strength distribution	241
		•	•	The induced asymmetrical open-circuit voltage distribution	245
		,	•	The outlet-voltage distribution	248
		,	•	Some mathematical relations	240 250
		•	,		250
		`	,	Harmonic fields radiated at elevated angles from 27 MHz ISM round	252
					258
Fig	ure 1	– Relati	ve res	sponse of various detectors to impulse interference	22
Fig	ure 2	– Pulse	rectif	ication coefficient $P(\alpha)$	23
Fig	ure 3	– Pulse	repet	ition frequency	24
Fig	ure 4	– Block	diagra	am and waveforms of a simulator generating noise bursts	30
		– Block		am of a simulator generating noise bursts according to the pulse	31
Fig	ure 6	– Detail	s of a	typical output stage	32
ver	sus th	e calcul	ated o	of the measured outdoor magnetic field strength $H_{\rm O}$ (dB $\mu$ A/m) outdoor magnetic field strength $H_{\rm C}$ dB( $\mu$ A/m)	36
Fig	ure 8/	✓ Meası	ured o	outdoor magnetic versus distance, and probability of the building-	37
Fig	ure 9	– Norma	al prol	pability plot of the building-effect parameter Ab dB	38
Fig	ure 10	– Scat	ter plo	ot of the outdoor antenna factor $G_{O}$ dB( $\Omega$ m) versus the indoor	
			•	obability plots of the antenna factors	
				obability plot of the equivalent asymmetrical resistance $R_{f a}$ dB( $\Omega$ )	
				of the frequency dependence of some parameters	
_			-	If the frequency histogram $\Delta N(E_{\rm O}, \Delta E_{\rm O})$	
				• •	49
ma	ximum	ı field st	rengtl	of $n_{\rm m}(E_{\rm O})$ , i.e. the distribution of the outlets experiencing a h $E_{\rm O}$ resulting from a given number of transmitters in (or near) obtical region	50
				of the number of outlets with an induced asymmetrical open- $1 \le U_{\mbox{max}} = 79 \ \mbox{V}$ (see Table 10)	52
				of number (left-hand scale) and relative number (right-hand	
sca	le) of	outlets	with $I$	$U_{L} \leq U_{h} \leq U_{max}$	53

Figure 18 – Vertical polar patterns of horizontally polarized $E_x$ field strengths emitted around small vertical loop (horizontal magnetic dipole) over three different types of real ground
Figure 19 – Height scan patterns of vertically oriented $E_z$ field strengths emitted from small vertical loop (horizontal magnetic dipole) over three different types of real ground61
Figure 20 – Vertical polar patterns of horizontally polarized $E_{\chi}$ field strengths emitted around small vertical loop (horizontal magnetic dipole), over three different types of real ground
Figure 21 – Vertical polar patterns of vertically oriented $E_Z$ field strengths emitted around small vertical loop (horizontal magnetic dipole) over three different types of real ground
Figure 22 – Height scan patterns of vertically oriented $E_z$ field strengths emitted at 1 000 MHz from the small vertical loop (horizontal magnetic dipole), at horizontal distance of 10 m, 30 m and 300 m in the Z-X plane over three different types of real ground
Figure 23 – Vertical polar patterns of horizontally polarized $E_{\chi}$ and vertically oriented $E_{z}$ field strengths emitted around small horizontal electric dipole, in Y-Z and Z-X planes respectively
Figure 24 – Height scan patterns of horizontally polarized E field strengths emitted from small horizontal electric dipole
Figure 25 – Vertical polar patterns of horizontally polarized $E_z$ and vertically oriented $E_z$ field strengths emitted around small horizontal electric dipole in $Y$ -Z and Z-X planes respectively
Figure 26 – Height scan patterns of horizontally polarized $E_{\chi}$ field strengths emitted small horizontal electric dipole
Figure 27 – Vertical polar patterns of horizontally polarized $E_{\chi}$ and vertically oriented $E_{z}$ field strengths emitted around small vertical loop (porizontal magnetic dipole) in Y-Z and Z-X planes respectively
Figure 28 – Height scan patterns of vertically oriented $E_z$ and horizontally oriented $E_x$ field strengths emitted from small vertical loop (horizontal magnetic dipole)70
Figure 29 – Vertical polar patterns of vertically oriented $E_z$ and horizontally oriented $E_x$ field strengths emitted around small vertical electric dipole73
Figure 30 – Height scan patterns of vertically oriented $E_z$ and horizontally oriented $E_x$ field strengths emitted from small vertical electric dipole73
Figure 31 – Vertical polar patterns of horizontally polarized $E_X$ and vertically oriented $E_Z$ field strengths emitted around small vertical loop (horizontal magnetic dipole) in Y-Z and Z-X planes respectively
Figure 32 – Height scan patterns of vertically oriented $E_z$ and horizontally oriented $E_x$ field strengths emitted from small vertical loop (horizontal magnetic dipole)74
Figure 33 – Vertical polar patterns of horizontally polarized <i>E</i> -field strength emitted around small horizontal loop (vertical magnetic dipole)
Figure 34 – Height scan patterns of horizontally polarized <i>E</i> -field strength emitted from small horizontal loop (vertical magnetic dipole)75
Figure 35 – Vertical polar patterns of vertically oriented $E_{\mathcal{Z}}$ and horizontally oriented $E_{\mathcal{X}}$ field strengths emitted around small vertical electric dipole78
Figure 36 – Height scan patterns of vertically oriented $E_z$ and horizontally oriented $E_x$ field strengths emitted from the small vertical electric dipole
Figure 37 – Vertical polar patterns of horizontally polarized $E_\chi$ and vertically oriented $E_Z$ field strengths emitted around small vertical loop (horizontal magnetic dipole) in Y-Z and Z-X planes respectively79
Figure 38 – Height scan patterns of vertically oriented $E_z$ and horizontally oriented $E_x$ field strengths emitted from small vertical loop (horizontal magnetic dipole)

Figure 39 – Vertical polar patterns of horizontally polarized <i>E</i> -field strength emitted around small horizontal loop (vertical magnetic dipole)	80
Figure 40 – Height scan patterns of horizontally polarized <i>E</i> -field strength emitted from small horizontal loop (vertical magnetic dipole)	80
Figure 41 – Vertical polar patterns of horizontally polarized <i>E</i> -field strength emitted around the small horizontal loop (vertical magnetic dipole)	83
Figure 42 – Height scan patterns of horizontally polarized <i>E</i> -field strength emitted from small horizontal loop (vertical magnetic dipole)	83
Figure 43 – Height scan patterns of horizontally polarized $\it E$ -field strength emitted from small horizontal loop (vertical magnetic dipole)	. 87
Figure 44 – Height scan patterns of the vertical component of the <i>E</i> -fields emitted from a small vertical electric dipole	. 90
Figure 45 – Height scan patterns of the vertical component of the <i>E</i> -fields entitled from a small vertical electric dipole	. 90
Figure 46 – Height scan patterns of the horizontally polarized E fields emitted in the vertical plane normal to the axis of a small horizontal electric dipole	92
Figure 47 – Height scan patterns of the horizontally polarized E-fields emitted in the vertical plane normal to the axis of a small horizontal electric dipole	92
Figure 48 – Ranges of uncertainties in the predictability of radiation in vertical directions from electrically small sources located at a height of 1 m or 2 m above ground	. 94
Figure 49 – Ranges of uncertainties in the predictability of radiation in vertical directions from electrically small sources located at a height of 1 m or 2 m above ground	. 95
Figure 50 – Ranges of uncertainties in the predictability of radiation in vertical directions from electrically small sources located at a height of 1 m or 2 m above ground	. 96
Figure 51 – Geometry of the small vertical electric dipole model	100
Figure 52 - Geometry of the small horizontal electrical dipole model	100
Figure 53 – Geometry of the small horizontal magnetic dipole model (small vertical loop)	100
Figure 54 – Geometry of the small vertical magnetic dipole model (small horizontal loop)	100
Figure 55 – Ranges of errors in the predictability of radiation in vertical directions from electrically small sources located close to the ground, based on measurements of the horizontally oriented X-field near ground at a distance of 30 m from the sources	108
Figure 56 – Ranges of errors in the predictability of radiation in vertical directions from electrically small sources located close to the ground, based on measurements of the horizontally oriented <i>H</i> -field at the ground supplemented with measurements of the vertically oriented <i>H</i> -field in a height scan up to 6 m at a distance of 30 m from the sources.	109
Figure 57 – Vertical radiation patterns of horizontally oriented <i>H</i> -fields emitted by a small vertical electric dipole located close to the ground	
Figure 58 – Vertical radiation patterns of horizontally oriented <i>H</i> -fields emitted by a small vertical electric dipole located close to the ground	111
Figure 59 – Vertical radiation patterns of <i>E</i> -fields emitted by a small vertical electric dipole located close to the ground	112
Figure 60 – Vertical radiation patterns of the <i>E</i> -fields emitted by a small vertical electric dipole located close to the ground	112
Figure 61 – Vertical radiation patterns of the <i>H</i> -fields emitted by a small horizontal electric dipole located close to the ground	113

Figure 62 – Influence of a wide range of values of the electrical constants of the ground on the vertical radiation patterns of the horizontally oriented <i>H</i> -fields emitted by a small horizontal electric dipole located close to the ground	3
Figure 63 – Vertical radiation patterns of the horizontally oriented <i>H</i> -fields emitted by a small horizontal electric dipole located close to the ground	4
Figure 64 – Vertical radiation patterns of the <i>E</i> -fields emitted by a small horizontal electric dipole located close to the ground	4
Figure 65 – Vertical radiation patterns of the <i>E</i> -fields emitted by a small horizontal electric dipole located close to the ground	5
Figure 66 – Vertical radiation patterns of <i>H</i> -fields emitted by small horizontal magnetic dipole (vertical loop) located close to ground11:	5
Figure 67 – Vertical radiation patterns of the horizontally oriented <i>H</i> -fields emitted by a small horizontal magnetic dipole (vertical loop) located close to the ground110	6
Figure 68 – Vertical radiation patterns of the horizontally oriented <i>H</i> fields emitted by a small horizontal magnetic dipole (vertical loop) located close to the ground110	6
Figure 69 – Vertical radiation patterns of the <i>E</i> -fields emitted by a small horizontal magnetic dipole (vertical loop) located close to the ground	7
Figure 70 – Vertical radiation patterns of the <i>E</i> -fields emitted by a small horizontal magnetic dipole (vertical loop) located close to the ground	7
Figure 71 – Vertical radiation patterns of the <i>H</i> -fields emitted by a small vertical magnetic dipole (horizontal loop) located close to the ground	8
Figure 72 – Vertical radiation patterns of the H fields emitted by a small vertical magnetic dipole (horizontal loop) located close to the ground	8
Figure 73 – Vertical radiation patterns of the <i>H</i> -fields emitted by a small vertical magnetic dipole (horizontal loop) located close to the ground	9
Figure 74 – Vertical radiation patterns of the H-fields emitted by a small vertical magnetic dipole (horizontal loop) located close to the ground	9
Figure 75 – Vertical radiation pattern of the E field emitted by a small vertical magnetic dipole (horizontal loop) located close to the ground	0
Figure 76 – Vertical radiation patterns of the <i>E</i> -fields emitted by a small vertical magnetic dipole (horizontal loop) located close to the ground	0
Figure 77 – Vertical radiation patterns of the horizontally oriented <i>H</i> -fields emitted by a small vertical electric dipole located close to the ground	1
Figure 78 – Vertical radiation patterns of the <i>E</i> -fields emitted by a small vertical electric dipole located close to the ground	1
Figure 79 – Vertical radiation patterns of the <i>E</i> -fields emitted by a small vertical electric dipole located close to the ground	2
Figure 80 – Vertical radiation patterns of the <i>H</i> -fields emitted by a small horizontal electric dipole located close to the ground	2
Figure 81 – Vertical radiation patterns of the horizontally oriented <i>H</i> -fields emitted by a small horizontal electric dipole located close to the ground	3
Figure 82 – Vertical radiation patterns of the <i>E</i> -fields emitted by a small horizontal electric dipole located close to the ground	3
Figure 83 – Vertical radiation patterns of the <i>E</i> -fields emitted by a small horizontal electric dipole located close to the ground	4
Figure 84 – Vertical radiation patterns of the <i>H</i> -fields emitted by a small horizontal magnetic dipole (vertical loop) located close to the ground	4
Figure 85 – Vertical radiation patterns of the horizontally oriented <i>H</i> -fields emitted by a small horizontal magnetic dipole (vertical loop) located close to the ground	5
Figure 86 – Vertical radiation patterns of the horizontally oriented <i>H</i> -fields emitted by a small horizontal magnetic dipole (vertical loop) located close to the ground	5

Figure 87 – Vertical radiation patterns of the <i>E</i> -fields emitted by a small horizontal magnetic dipole (vertical loop) located close to the ground	126
Figure 88 – Vertical radiation patterns of the <i>E</i> -fields emitted by a small horizontal magnetic dipole (vertical loop) located close to the ground	126
Figure 89 – Vertical radiation patterns of the <i>H</i> -fields emitted by a small vertical magnetic dipole (horizontal loop) located close to the ground	127
Figure 90 – Vertical radiation patterns of the <i>H</i> -fields emitted by a small vertical magnetic dipole (horizontal loop) located close to the ground	127
Figure 91 – Vertical radiation patterns of the <i>H</i> -fields emitted by a small vertical magnetic dipole (horizontal loop) located close to the ground	128
Figure 92 – Vertical radiation patterns of the <i>E</i> -fields emitted by a small vertical magnetic dipole (horizontal loop) located close to the ground	128
Figure 93 – Vertical radiation patterns of the horizontally oriented <i>H</i> -fields emitted by a small vertical electric dipole located close to the ground	129
Figure 94 – Vertical radiation patterns of the <i>E</i> -fields emitted by a small vertical electric dipole located close to the ground	129
Figure 95 – Vertical radiation patterns of the <i>E</i> -fields emitted by a small vertical electric dipole located close to the ground	130
Figure 96 – Vertical radiation patterns of the <i>H</i> -fields emitted by a small horizontal electric dipole located close to the ground	130
Figure 97 – Vertical radiation patterns of the Effields emitted by a small horizontal electric dipole located close to the ground	131
Figure 98 – Vertical radiation patterns of the <i>E</i> -fields emitted by a small horizontal electric dipole located close to the ground	131
Figure 99 – Vertical radiation patterns of the <i>H</i> -field emitted by a small horizontal magnetic dipole (vertical loop) located close to the ground	132
Figure 100 – Vertical radiation patterns of the vertically polarized <i>E</i> -fields emitted by a small horizontal magnetic dipole (vertical loop) located close to the ground	132
Figure 101 – Vertical radiation patterns of the <i>H</i> -field emitted by a small vertical magnetic dipole (horizontal loop) located close to the ground	
Figure 102 – Vertical radiation patterns of the <i>E</i> -fields emitted by a small vertical magnetic dipole (horizontal loop) located close to the ground	
Figure 103 – Vertical radiation patterns of the horizontally oriented <i>H</i> -fields emitted by a small vertical electric dipole located close to the ground	
Figure 104 Vertical radiation patterns of the vertically polarized <i>E</i> -fields emitted by a small vertical electric dipole located close to the ground	134
Figure 105 – Vertical radiation patterns of the <i>H</i> -fields emitted by a small horizontal electric dipole located close to the ground	
Figure 106 – Vertical radiation patterns of the horizontally oriented <i>H</i> -fields emitted by a small horizontal electric dipole located close to the ground	
Figure 107 – Influence of a wide range of values of the electrical constants of the ground on the vertical radiation patterns of the horizontally oriented <i>H</i> -fields emitted by a small horizontal electric dipole located close to the ground	136
Figure 108 – Vertical radiation patterns of the vertically polarized <i>E</i> -fields emitted by a small horizontal electric dipole located close to the ground	136
Figure 109 – Vertical radiation patterns of the <i>H</i> -fields emitted by a small horizontal magnetic dipole (vertical loop) located close to the ground	137
Figure 110 – Vertical radiation patterns of the vertically polarized <i>E</i> -fields emitted by a small horizontal magnetic dipole (vertical loop) located close to the ground	137
Figure 111 – Vertical radiation patterns of the <i>H</i> -fields emitted by a small vertical magnetic dipole (horizontal loop) located close to the ground	138

Figure 112 – Vertical radiation patterns of the <i>E</i> -fields emitted by a small vertical magnetic dipole (horizontal loop) located close to the ground	138
Figure 113 – Set-up for measuring communication quality degradation of a wireless	139
Figure 114 – APD characteristics of disturbance	141
Figure 115 – Wireless LAN throughput influenced by noise	142
Figure 116 – Set-up for measuring the communication quality degradation of Bluetooth	
Figure 117 – APD of disturbance of actual MWO (2 441MHz)	
Figure 118 – APD characteristics of disturbance (2 460 MHz)	144
Figure 119 – Throughput of Bluetooth influenced by noise	146
Figure 120 – Set-up for measuring the BER of W-CDMA	147
Figure 121 – APD characteristics of disturbance	148
Figure 122 – BER of W-CDMA caused by radiation noise	149
Figure 123 – Set-up for measuring the PHS throughput	150
Figure 124 – Set-up for measuring the BER of PHS	150
Figure 125 – APD characteristics of disturbance	151
Figure 126 – PHS throughput caused by radiation	152
Figure 127 – BER of PHS caused by radiation noise	153
Figure 128 – Correlation of the disturbance voltages with the system performance $(C/N_0)$	154
Figure 129 – Correlation of the disturbance voltages with the system performance	155
Figure 130 – Correlation of the disturbance voltages with the system performance	155
Figure 131 – Correlation of the disturbance voltages with the system performance (C/N <sub>0</sub> )	156
Figure 132 – Correlation of the disturbance voltages with the system performance $(C/N_0)$	156
Figure 133 – Experimental set-up for measuring communication quality degradation of a PHS or W-CDMA	157
Figure 134 – Simulation set-up for estimating communication quality degradation of a PHS or W-CDMA	157
Figure 135 - APD of pulse disturbance	158
Figure 136 - BER degradation of PHS and W-CDMA caused by repetition pulse (Carrier power, -35 dBm)	158
Figure 137 – Evaluation method of the correlation between BER and APD	159
Figure 138 – Correlation between measured $\Delta$ $L_{\sf BER}$ and $\Delta$ $L_{\sf APD}$	159
Figure 139 – Correlation between measured $p_{BER}$ and $p_{APD}$	160
Figure 140 – Weighting curves of quasi-peak measuring receivers for the different frequency ranges as defined in CISPR 16-1-1	161
Figure 141 – Weighting curves for peak, quasi-peak, rms and linear average detectors for CISPR bands C and D	162
Figure 142 – Test setup for the measurement of the pulse weighting characteristics of a digital radiocommunication system	163
Figure 143 – Example of an interference spectrum: pulse modulated carrier with a pulse duration of 0,2 μs and a PRF < 10 kHz	164
Figure 144 – The rms and peak levels for constant BEP for three $K = 3$ , convolutional	400

Figure 145 – The rms and peak levels for constant BEP for two rate ½, convolutional code	167
Figure 146 – Test setup for the measurement of weighting curves for Digital Radio Mondiale (DRM)	169
Figure 147 – Weighting characteristics for DRM signals for various pulse widths of the pulse-modulated carrier	170
Figure 148 – Weighting characteristics for DRM protection level 0: average of results for two receivers	171
Figure 149 – Weighting characteristics for DRM protection level 1: average of results for two receivers	171
Figure 150 – Weighting characteristics for DVB-T with 64 QAM 2k, CR 3/4 (as used in France and UK)	173
Figure 151 – Weighting characteristics for DVB-T with 64 QAM 8k, CR 3/4 (as used in Spain)	174
Figure 152 – Weighting characteristics for DVB-T with 16 QAM 8k, CR 2/3 (as used in Germany)	174
Figure 153 – Average weighting characteristics of 6 receiver types for DVB-T with 16QAM	175
Figure 154 – Average weighting characteristics of 6 (eceiver types for DVB-T with 64QAM	176
Figure 155 – Weighting characteristics for DAB (signal level -71 dBm) with a flat response down to approximately 1 kHz	177
Figure 156 – Weighting characteristics for DAB: average of two different commercial receiver types	177
Figure 157 – Weighting characteristics for TETRA (signal level – 80 dBm) for a code rate of 1	178
Figure 158 - Weighting characteristics for RBER 1b of GSM (signal level -90 dBm)	179
Figure 159 – Weighting characteristics for RBER 2 of GSM	179
Figure 160 – Carrier-to-interference improvements with decreasing PRF in dB computed for GSM using COSSAP	180
Figure 161 – Rms and quasi-peak values of pulse level for constant effect on FM radio reception	180
Figure 162 - Weighting characteristics for RBER 1b of GSM (signal level -90 dBm)	181
Figure 163 - Weighting characteristics for DECT (signal level -83 dBm)	182
Figure 164 – Weighting characteristics for IS-95 (signal level -97 dBm) with comparatively high immunity to interference	183
Figure 165 – Weighting characteristics for J-STD 008 (signal level –97 dBm)	183
Figure 166 – Weighting characteristics for the Frame Error Ratio (FER) of CDMA2000 (measured at a receive signal level of -112 dBm) for a low data rate of 9,6 kb/s	184
Figure 167 – Weighting characteristics for the Frame Error Ratio (FER) of CDMA2000 (measured at a receive signal level of –106 dBm) for two different data rates (9,6 kb/s and 76,8 kb/s)	185
Figure 168 – The proposed rms-average detector for CISPR Bands C and D with a corner frequency of 100 Hz	188
Figure 169 – Rms-average detector function by using an rms detector followed by a linear average detector and peak reading	188
Figure 170 – Rms-average weighting functions for CISPR Bands A, B, C/D and E for the shortest pulse widths allowed by the measurement bandwidths	189

Figure 171 – Shift of the rms-average weighting function for CISPR band C/D by using a bandwidth of 1 MHz instead of 120 kHz, if the shortest possible pulse widths are applied	190
Figure 172 – Example of a simple EUT model	192
Figure 173 – Representation of a CMAD as a two-port device	194
Figure 174 – Conformal mapping between z-plane and f-plane	196
Figure 175 – Conversion from 50 $\Omega$ coaxial system to the geometry of the two-port device-under-test	198
Figure 176 – Basic model for the TRL calibration	199
Figure 177 – The four calibration configurations necessary for the TRL calibration	200
Figure 178 – Measurement of CMAD characteristics	204
Figure 179 – Preliminary measurements of the test set-up	206
Figure 180 – Position of the reference planes for the measurement with SQLT calibration and $ABCD$ transformation to $Z_{\text{ref}}$ level	207
Figure 181 – Superheterodyne EMI receiver	209
Figure 182 – An example spectrogram $Z[m,k]$	211
Figure 183 – Sidelobe effect due to the finite length of window	213
Figure 184 – Measurement error for a single pulse	214
Figure 185 – IF signal for different overlapping factors for the same sequence of pulses	215
Figure 186 – FFT-based baseband system	216
Figure 187 - Real-time FFT-based measuring instrument	217
Figure 188 – Digital down converter	217
Figure 189 - Short time fast Fourier transform - An example of implementation	218
Figure 190 - Floating-point analogue-to-digital conversion	218
Figure 191 - Example of a 120 kHz Gaussian filter	219
Figure 192 - Essential parts of an FFT-based heterodyne receiver	220
Figure 193 – Dynamic range for broadband emission as measured with the peak detector	222
Figure 194 - Set-up of FFT-based system type 2	222
Figure 195 - FFT Software ("FFTemi") screen shot	225
Figure 196 - Example of pulse generator measurement with antenna	226
Figure 197 - Radiated emission measurement of a motor - peak detector	227
Figure 198 – Angular characterization of a PC	227
Figure 199 – Example FFT IF analysis display	228
Figure A.1 – Example plot using the expression $P_t + G = P_q + 2$	238
Figure A.2 – Examples of a number of microwaves measured for $P_q$ and $P_t$	240
Figure B.1 – Definition of the ring-shaped area round the transmitter T	242
Figure C.1 – The permissible ranges of $U_h$ and $G$ are within the polygon $\{G_L, U_a\}$ , $\{G_L, U_b\}$ , $\{G_L, U_d\}$ , $\{G_I, U_C\}$ and $\{G_L, U_a\}$ . For the given value $U_L$ the double-shaded area represents $pr\{U_h \geq U_L\}$	246
Figure F.1 – Vertical radiation patterns of horizontally polarized fields, 109 MHz, 300 m scan radius (adapted from [34])	
Figure F.2 – Vertical radiation patterns of horizontally polarized fields, 109 MHz, 300 m scan radius (adapted from [34])	255

Figure F.3 – Vertical radiation patterns of horizontally polarized fields, 109 MHz, 300 m scan radius (adapted from [34])	256
Figure F.4 – Vertical radiation patterns of horizontally polarized fields, 109 MHz, 300 m scan radius (adapted from [34])	257
Table 1 – Comparative response of slideback peak, quasi-peak and average detectors to sine wave, periodic pulse and Gaussian waveform	22
Table 2 – Characteristics of gate generator and modulator to simulate various types of broadband interference	28
Table 3 – Summary results of building-effect, A <sub>b</sub> , analysis	38
Table 4 – Summary of results of <i>G</i> -factor analysis	41
Table 5 – Summary of L <sub>O</sub> factors (far-field)	41
Table 6 – Summary of truncation parameters of $f(G)$	42
Table 7 – Summary results of equivalent-resistance analysis	43
Table 8 – Example of field-strength classification	46
Table 9 – Example of voltage classification assuming for the outdoor field strength: $E_{\text{max}} = 60 \text{ V/m}$ and $E_{\text{min}} = 0.01 \text{ V/m}$	47
Table 10 – Summary of the parameters used in the numerical examples presented in Figures 16 and 17	51
Table 11 – Frequencies of interest in ITU designated bands from Table 9 of CISPR 11:2009	58
Table 12 – Electrical constants for "medium dry ground" [31] (CCIR: medium dry ground; rocks; sand; medium sized towns[32])	59
Table 13 – Electrical constants for "wet ground" [31] (CCIR: marshes (fresh water); cultivated land [24]) and "very dry ground" [31] (CCIR: very dry ground; granite mountains in cold regions; industrial areas [32])	59
Table 14 – Estimates of the errors in prediction of radiation in vertical directions based on a measurement height scan from 1 m to 4 m at known distances, d; frequency = 75 MHz (adapted from [39])	67
Table 15 – Estimates of the errors in prediction of radiation in vertical directions based on a measurement height scan from 1 m to 4 m at known distances, d; frequency = 110 MHz (adapted from [39])	71
Table 16 — Estimates of the errors in prediction of radiation in vertical directions based on a measurement height scan from 1 m to 4 m at known distances, d; frequency = 243 MHz (adapted from [39])	
Table 17 – Estimates of the errors in prediction of radiation in vertical directions based on a measurement height scan from 1 m to 4 m at known distances, d; frequency = 330 MHz (adapted from [39])	
Table 18 – Estimates of the errors in prediction of radiation in vertical directions based on a measurement height scan from 1 m to 4 m at known distances, $d$ ; frequency = 1 000 MHz (adapted from [39])	84
Table 19 – Predictability of radiation in vertical directions at 100 kHz, using ground-based measurements of horizontally oriented <i>H</i> -field at distances up to 3 km from the source (figures are located in 4.6.8)	101
Table 20 – Predictability of radiation in vertical directions at 1 MHz, using ground-based measurements of horizontally oriented <i>H</i> -field at distances up to 300 m from the source (figures are located in 4.6.8)	103
Table 21 – Predictability of radiation in vertical directions at 10 MHz, using ground-based measurements of horizontally oriented <i>H</i> -field at distances up to 300 m from the source (figures are located in 4.6.8)	104

Table 22 – Predictability of radiation in vertical directions at 30 MHz, using ground- based measurements of horizontally oriented <i>H</i> -field at distances up to 300 m from the source (figures are located in 4.6.8)	105
(.9)	
Table 23 – Conditions for measuring communication quality degradation	
Table 24 – Average and rms values of noise level normalized by $N_0$	
Table 25 – Conditions for measuring communication quality degradation of Bluetooth	
Table 26 – Average and rms values of noise level normalized by $N_0$	
Table 27 – Average and rms values of noise level normalized by $N_0$	. 145
Table 28 – Conditions for measuring communication quality degradation of W-CDMA	. 147
Table 29 – Average and rms values of noise level normalized by $N_0$	. 148
Table 30 – Conditions for measuring the PHS throughput	. 150
Table 31 – Conditions for measuring the BER of PHS	. 150
Table 32 – Average and rms values of noise level normalized by $N_0$	. 151
Table 33 – Overview of types of interference used in the experimental study of weighting characteristics	. 164
Table 34 – DRM radio stations received for the measurement of the weighting characteristics	. 168
Table 35 – Comparison of BER values for the same interference level	. 172
Table 36 – Transmission parameters of DVB-T systems used in various countries	
Table 37 – Example of measurement results in dB(μV) of unmodulated and FM modulated carriers for various detectors (bandwidth 120 kHz)	. 186
Table 38 – Survey of the corner frequencies found in the various measurement results	. 187
Table 39 – Measurement results for broadband disturbance sources (measurements with rms-average and quasi-peak detectors are normalized to average detector values)	. 191
Table 40 – Expected deviations between different laboratories for small EUTs due to variations of the impedance Zapparent at point B	. 192
Table 41 – Calibration measurement results format	. 201
Table 42 – Scan times	. 219
Table 43 – Sampling rates for different BWIF	. 223
Table 44 – Scan times for a scap 30 MHz to 1 GHz	. 224

#### INTERNATIONAL ELECTROTECHNICAL COMMISSION

### SPECIFICATION FOR RADIO DISTURBANCE AND IMMUNITY MEASURING APPARATUS AND METHODS –

#### Part 3: CISPR technical reports

#### **FOREWORD**

- 1) The International Electrotechnical Commission (IEC) is a worldwide organization for standardization comprising all national electrotechnical committees (IEC National Committees). The object of IEC is to promote international co-operation on all questions concerning standardization in the electrical and electronic tields. To this end and in addition to other activities, IEC publishes International Standards, Technical Specifications, Technical Reports, Publicly Available Specifications (PAS) and Guides (hereafter referred to as "IEC Publication(s)"). Their preparation is entrusted to technical committees; any IEC National Committee interested in the subject dealt with may participate in this preparatory work. International, governmental and non-governmental organizations liaising with the IEC also participate in this preparation. IEC collaborates closely with the International Organization for Standardization (ISO) in accordance with conditions determined by agreement between the two organizations.
- 2) The formal decisions or agreements of IEC on technical matters express, as nearly as possible, an international consensus of opinion on the relevant subjects since each technical committee has representation from all interested IEC National Committees.
- 3) IEC Publications have the form of recommendations for international use and are accepted by IEC National Committees in that sense. While all reasonable efforts are made to ensure that the technical content of IEC Publications is accurate, IEC cannot be held responsible for the way in which they are used or for any misinterpretation by any end user.
- 4) In order to promote international uniformity, IEC National Committees undertake to apply IEC Publications transparently to the maximum extent possible in their national and regional publications. Any divergence between any IEC Publication and the corresponding national or regional publication shall be clearly indicated in the latter.
- 5) IEC itself does not provide any attestation of conformity. Independent certification bodies provide conformity assessment services and in some areas, access to IEC marks of conformity. IEC is not responsible for any services carried out by independent certification bodies.
- 6) All users should ensure that they have the latest edition of this publication.
- 7) No liability shall attach to IEC or its directors, employees, servants or agents including individual experts and members of its technical committees and IEC National Committees for any personal injury, property damage or other damage of any nature whatsoever, whether direct or indirect, or for costs (including legal fees) and expenses arising out of the publication, use of, or reliance upon, this IEC Publication or any other IEC Publications.
- 8) Attention is drawn to the Normative references cited in this publication. Use of the referenced publications is indispensable for the correct application of this publication.
- 9) Attention is drawn to the possibility that some of the elements of this IEC Publication may be the subject of patent rights. IEC sharl not be held responsible for identifying any or all such patent rights.

This consolidated version of CISPR 16-3 consists of the third edition (2010) [documents CISPR/A/888/DTR and CISPR/A/899/RVC and its amendment 1 (2012) [documents CISPR/A/975/DTR and CISPR/A/996/RVC]. It bears the edition number 3.1.

The technical content is therefore identical to the base edition and its amendment and has been prepared for user convenience. A vertical line in the margin shows where the base publication has been modified by amendment 1. Additions and deletions are displayed in red, with deletions being struck through.

The main task of IEC technical committees is to prepare International Standards. However, a technical committee may propose the publication of a technical report when it has collected data of a different kind from that which is normally published as an International Standard, for example "state of the art."

CISPR 16-3, which is a technical report, has been prepared by CISPR subcommittee A: Radio-interference measurements and statistical methods.

The main technical change with respect to the previous edition consist of the addition of a new clause to provide background information on FFT instrumentation.

A list of all parts of the CISPR 16 series can be found, under the general title Specification for radio disturbance and immunity measuring apparatus and methods, on the IEC website.

This publication has been drafted in accordance with the ISO/IEC Directives, Part 2.

The committee has decided that the contents of the base publication and its amendments will remain unchanged until the stability date indicated on the IEC web site under "http://webstore.iec.ch" in the data related to the specific publication. At this date, the publication will be

- reconfirmed,
- · withdrawn,
- replaced by a revised edition, or
- · amended.

A bilingual version of this publication may be issued at a later date.

IMPORTANT – The colour inside logo on the cover page of this publication indicates that it contains colours which are considered to be useful for the correct understanding of its contents. Users should therefore print this document using a colour printer.

# SPECIFICATION FOR RADIO DISTURBANCE AND IMMUNITY MEASURING APPARATUS AND METHODS –

#### Part 3: CISPR technical reports

#### 1 Scope

This part of CISPR 16 is a collection of technical reports (Clause 4) that serve as background and supporting information for the various other standards and technical reports in CISPR 16 series. In addition, background information is provided on the history of CISPR, as well as a historical reference on the measurement of interference power from household and similar appliances in the VHF range (Clause 5).

Over the years, CISPR prepared a number of recommendations and reports that have significant technical merit but were not generally available. Reports and recommendations were for some time published in CISPR 7 and CISPR 8.

At its meeting in Campinas, Brazil, in 1988, CISPR subcommittee A agreed on the table of contents of Part 3, and to publish the reports for posterity by giving the reports a permanent place in Part 3.

With the reorganization of CISPR 16 in 2003, the significance of CISPR limits material was moved to CISPR 16-4-3, whereas recommendations on statistics of disturbance complaints and on the report on the determination of limits were moved to CISPR 16-4-4. The contents of Amendment 1 (2002) of CISPR 16-3 were moved to CISPR 16-4-1.

NOTE As a consolidated collection of independent technical reports, this document may contain symbols that have differing meanings from one clause to the next. Attempts have been made to minimize this to the extent possible at the time of editing.

#### 2 Normative references

The following referenced documents are indispensable for the application of this document. For dated references, only the edition cited applies. For undated references, the latest edition of the referenced document (including any amendments) applies.

CISPR 11:2009, Industrial, scientific and medical equipment – Radio-frequency disturbance characteristics – Limits and methods of measurement

CISPR 16-1-1, Specification for radio disturbance and immunity measuring apparatus and methods – Part 1-1: Radio disturbance and immunity measuring apparatus – Measuring apparatus

IEC 60050-161:1990, International Electrotechnical Vocabulary (IEV) – Chapter 161: Electromagnetic compatibility

IEC 60050-300:2001, International Electrotechnical Vocabulary (IEV) – Electrical and electronic measurements and measuring instruments – Part 311: General terms relating to measurements – Part 312: General terms relating to electrical measurements – Part 313: Types of electrical measuring instruments – Part 314: Specific terms according to the type of instrument

ISO/IEC Guide 99:2007, International vocabulary of metrology – Basic and general concepts and associated terms (VIM)